

Forecasting Patient Outcomes in Kidney Exchange

Naveen Durvasula¹, John Dickerson² and Aravind Srinivasan²

¹University of California, Berkeley

²University of Maryland, College Park

ndurvasula@berkeley.edu {john, srin}@cs.umd.edu,

Abstract

Kidney exchanges allow patients with end-stage renal disease to find a lifesaving living donor by way of an organized market. However, not all patients are equally easy to match, nor are all donor organs of equal quality—some patients are matched within weeks, while others may wait for years with no match offers at all. We propose the first decision-support tool for kidney exchange that takes as input the biological features of a patient-donor pair, and returns (i) the probability of being matched prior to expiry, and (conditioned on a match outcome), (ii) the waiting time for and (iii) the organ quality of the matched transplant. This information may be used to inform medical and insurance decisions. We predict all quantities (i, ii, iii) exclusively from match records that are readily available in any kidney exchange using a quantile random forest approach. To evaluate our approach, we developed two state-of-the-art realistic simulators based on data from the United Network for Organ Sharing that sample from the training and test distribution for these learning tasks—in our application these distributions are distinct. We analyze distributional shift through a theoretical lens, and show that the two distributions converge as the kidney exchange nears steady-state. We then show that our approach produces clinically-promising estimates using simulated data. Finally, we show how our approach, in conjunction with tools from the model explainability literature, can be used to calibrate and detect bias in matching policies.

1 Introduction

Renal disease affects millions of people worldwide, with a societal burden comparable to diabetes [Neuen *et al.*, 2013]. A patient with end-stage renal failure requires one of two treatments to stay alive: frequent and costly filtration and replacement of their blood (dialysis), or the reception of an organ transplant from a donor with one or more healthy kidneys. The latter option is often preferable due to increased quality of life and other health outcomes [Santos *et al.*, 2015]. Donor kidneys are obtained from one of three sources: the deceased

donor waiting list, where cadaveric kidneys are harvested from deceased donors with still-healthy kidneys; ad-hoc arrangements between a compatible living donor and a patient; and, recently, *kidney exchanges* – an organized market where patients swap willing donors with other patients [Roth *et al.*, 2004; Roth *et al.*, 2005a; Roth *et al.*, 2005b]. Kidney exchanges, while still quite new, result in increased numbers and quality of transplants [Sönmez *et al.*, 2017];

The act of getting a kidney transplant is time-sensitive, and affects healthcare and lifestyle decisions; furthermore, the expected quality of the kidney—if any—received by a patient affects the decision to accept or reject a particular match offer. Thus, decision-support systems that incorporate donor and patient features and quantify or predict the value of a current or future offered kidney are valuable to practitioners. The Kidney Donor Profile Index (KDPI) [Rao *et al.*, 2009] and the Living Kidney Donor Profile Index (LKDPI) [Massie *et al.*, 2016] are well-known and used to assess deceased- and living-donor kidneys, respectively. However, no corresponding method (nor system) currently exists for future kidney exchange offers.

Although all transplants in kidney exchange systems are living-donor transplants, the LKDPI metric may not be applied directly in this domain, as unlike in standard ad-hoc living-donor donation, the features of the end donor are unknown and are generated through a stochastic matching process. Indeed, this stochasticity plays a large role in determining the value of a future kidney offer. Patients may or may not be matched due to random causes. Further, even if one conditions on a match outcome, the waiting time and quality of the transplant a patient ends up receiving is highly stochastic due to reasons we outline in Section 2. Thus, a successful decision-support system for kidney exchange must also quantify the variation that a patient should expect to face as opposed to simply giving point estimates.

We present four **principal contributions** in this paper.

- We give a random forest-based approach that takes as input features of a patient and their paired donor, and estimates (i) the probability of obtaining a match, and gives an estimate and prediction interval (e.g., 95% CI) for (ii) the quality of the match, and (iii) the waiting time of the match conditioned a match outcome. We validate our approach on real data from one of the largest fielded exchanges in the world.
- Our approach exclusively makes use of match records that

are routinely collected in any kidney exchange. One consequence that arises from using this data for prediction is that we encounter *distributional shift* – the features of patients who have exited the exchange may differ from those who have entered the exchange. We analyze this shift with a theoretical lens, and prove that it becomes negligible as the kidney exchange nears steady-state.

- We show how our approach may be adapted to provide kidney exchanges with a principled method for understanding how the current matching policy affects different types of patients. The economics literature suggests that certain patients may *never* be matched in a fully efficient matching due to their biological features (e.g. [Ashlagi and Roth, 2014; Toulis and Parkes, 2015]), motivating the design of *fair* policies. We use the Shapley Additive Explanation (SHAP) framework [Lundberg and Lee, 2017] to adapt our approach to provide consistent explanations for the variation in match outcomes as a function of the input features. Although SHAP analysis can be computationally intractable in the general case, a polynomial-time algorithm to compute SHAP values exists for RF models [Lundberg *et al.*, 2018]. Thus, our approach allows kidney exchanges to understand which populations are being treated unfairly by the current matching policy and by how much, and may therefore be used to calibrate patient prioritization.
- We provide a new state-of-the-art kidney exchange simulation framework capable of generating synthetic match records (a running list of the patients that have exited the exchange, along with their match outcomes), and patient trajectories (match outcomes for a specified patient upon being added to a specified pool). We believe that our framework can enable the research community to better understand the behavior of kidney exchanges, while protecting patient privacy, by providing a source of realistic synthetic data.

2 Preliminaries

The most-used model represents a kidney exchange as a directed graph that evolves over time $G(T) := (V(T), E(T))$, called a *compatibility graph*. Here, each patient and their paired donor who enter the pool are represented as a *single* vertex $v \in \mathcal{F}$ belonging to some *feature space* \mathcal{F} . Then, a directed edge is drawn from vertex v_i to vertex v_j if the patient at vertex v_j wants the donor kidney of vertex v_i . Edges are weighted by a function $w : \mathcal{F} \times \mathcal{F} \rightarrow \mathbb{R}$ that returns the utility of an individual kidney transplant represented by a directed edge (v_i, v_j) in terms of the features of the source and target nodes. In practice, these weights are used to (de)prioritize specific classes of patient [Dickerson *et al.*, 2014; UNOS, 2015].

Kidney exchanges rely on one of two types of structures to match patients: cycles and chains. First, a *k-cycle* c consists of exactly k patient-donor pairs (vertices), each connected by an edge in a cycle; here, each pair in c receives the kidney from the previous pair. Second, a *k-chain* begins with a non-directed donor, also known as an altruist, who enters the pool without a patient and gives their kidney to a patient with a paired donor, who gives to another patient with a paired

donor, and so on k times.¹

A *matching* M is a set of disjoint cycles and chains in a compatibility graph $G(T)$; $M \in \mathcal{M}(T)$, the set of all legal matchings at time $T \in [0, \infty)$. No donor can give more than one of her kidneys, necessitating the disjointness of cycles and chains. Given the set of all legal matchings $\mathcal{M}(T)$, the *clearing problem* finds the matching $M^*(T)$ that maximizes utility function $u : \mathcal{M}(T) \rightarrow \mathbb{R}$ (e.g., for maximum weighted matching, $u(M) = \sum_{c \in M} \sum_{(v_i, v_j) \in c} w(v_i, v_j)$). Formally: $M^* \in \arg \max_{M \in \mathcal{M}(T)} u(M)$. In practice, an integer program (IP) is used to compute $M^*(T)$ – these details and additional background on the kidney exchange can be found in Appendix A.

As the edges and edge weights are determined by the vertices in the pool through the weighting function w , the dynamics of the kidney exchange are driven by the dynamics of the vertex set $V(T)$. We may write these dynamics as $V(T) = (V(T-1) \cup A(T)) \setminus D(T) = \bigcup_{t=1}^T A(t) \setminus \bigcup_{t=1}^T D(t)$ for $T \in [1, \infty)$ with the initial condition $V(0) = \emptyset$, where $A(T) \subset \mathcal{F}$ and $D(T) \subset V(T) \cup A(T)$ denote the *arrivals* and *departures* at time T . The arrivals $A(T)$ consist of the new patients that entered the kidney exchange at time T , and the departures consist of patients that exited the pool at time T . Patients may exit the pool after a successful match, due to competition from other methods for receiving a kidney, or death (among other reasons). For every vertex $v \in D(T)$, we let the match outcome $O(v) \in \{0, 1\}$ denote whether or not the vertex was matched ($O(v) = 1$) or exited for other reasons ($O(v) = 0$). For any $v \in D(T)$ such that $O(v) = 1$, we let $W(v) = T - \min \{t \in [0, T] \mid v \in V(t)\}$ denote the *waiting time* for the vertex. We similarly define $Q(v) \in \mathbb{R}$ for such vertices as the LKDPI of the received transplant, as defined in Appendix A. The outcomes (O, W, Q) constitute the central learning targets in this paper.

In practice, the sets $A(T)$ and $D(T)$ are determined highly stochastically. In addition to the complexity introduced by the IP, in fielded kidney exchanges, matches are made without detailed knowledge of compatibility between a donor and patient. More-thorough physical *crossmatch tests* are done after an algorithmic match, but before the actual transplantation event, to ensure that a matched donor can donate to a paired patient. Even one failure of an edge in a cycle invalidates the *entire* cycle; similarly, given the incremental execution of chains, all potential transplants located after the first edge failure in a chain are invalidated. We simulate this complex dynamic process in our work; additional details are given in Section 4. This stochasticity, in addition to the dynamic nature of the kidney exchange, motivates the necessity to forecast the noise about patient outcomes.

3 Learning from Match Records

We aim to construct prediction intervals for the match outcome $O(v)$ in addition to the waiting time $W(v)$ and qual-

¹In fielded kidney exchanges, cycles are limited in size to, typically, 3; all surgeries in a cycle must be executed simultaneously, so longer cycles are nearly impossible to plan. Chains, however, can be much longer (or effectively endless) in practice.

ity $Q(v)$ conditioned on a match for a patient-donor pair that has just arrived in the pool. Every kidney exchange routinely keeps track of the patients who have arrived thus far in addition to the patients who have departed and their outcomes. Our central focus in this paper is demonstrating, both experimentally and theoretically, that this information can be used to forecast patient outcomes. Formally, we call this dataset $\mathcal{R}_T := \bigcup_{t=1}^T D(t)$, in conjunction with the outcomes $O(v), W(v), Q(v)$ for each $v \in \mathcal{R}_T$ the *match record* at time T , and we aim to predict the outcomes $O(v), W(v), Q(v)$ for new vertices $v \in A(T+1)$ that are about to *arrive*. Thus, there is an inherent distributional shift present in this learning task as the test distribution is given by the arrivals, but the training distribution is given by the departures, which have been filtered by the matching mechanism. We study the empirical and theoretical nature of this shift in subsequent sections.

3.1 Features and Categorical Encoding

We briefly describe the features we use for learning in our experiments. Our features correspond to the feature space \mathcal{F} used by the United Network for Organ Sharing, and should be adapted to correspond to the feature space of the target kidney exchange. Table 1 lists these features by data type.

Categorical	Donor/Patient Blood Type, Donor/Patient HLA
Boolean	Donor/Patient Sex [†] , Donor Race, Donor Cigarette Use [†]
Integer	Pool Size at Entry, Donor/Patient Age, Patient CPRA
Float	Donor/Patient Weight [‡] , Donor eGFR [‡] , Donor BMI, Donor Systolic BP

Table 1: **Data types of features used for prediction.** Features labeled by [†] are synthetically generated independently of other features. Features labeled by [‡] are synthetically generated, but drawn conditionally based on a combination of other synthetically generated and real features. All other features are generated from real data.

We encode the categorical features as follows. We make two Boolean features REC_A and REC_B to encode the patient’s blood type, where REC_A indicates whether the patient can receive *A*-type blood, and REC_B indicates whether the patient can receive *B*-type blood. We similarly make the features DON_A and DON_B to encode the donor’s blood type, where DON_A indicates whether the donor can donate *A*-type blood, and DON_B indicates whether the donor can donate *B*-type blood. Our encoding for the donor and patient HLA is more complex. Rather than using a collection of Boolean features, we instead use collections of integer features corresponding to the frequency of the antigen in the observed match record \mathcal{R}_T . This encoding, in addition to other training/model details, is outlined in Appendix B.

3.2 A Random Forest Approach

We propose a simple random forest approach to predicting these quantities. In addition to the fact that random forests do not require extensive parameter tuning and are computationally efficient to train, they may also be interpreted efficiently using the SHAP framework [Lundberg and Lee, 2017; Lundberg *et al.*, 2018] – we explore this in more detail in Section 7. We aim to produce more than just point estimates for

$O(v), W(v),$ and $Q(v)$, as there can be considerable noise about these quantities due to the stochastic nature of the kidney exchange. We may accomplish this for classification task of predicting the outcome by training a random forest classifier to predict O , and subsequently returning a positive class probability \hat{O} generated by the statistics of the constituent trees. We may apply a similar approach to produce 95% prediction intervals \hat{W}_{95} and \hat{Q}_{95} for the waiting time and quality using quantile regression forests [Meinshausen and Ridgeway, 2006]. In the remainder of this paper, we build a theoretical and empirical framework to justify this approach.

4 Simulation

As alluded to in previous sections, we evaluate our approach through simulation. Our simulation framework consists of *two* simulators—the batch simulator and the trajectory simulator: these generate the training and test data respectively. To our knowledge, our simulators are the first to use real data from a kidney exchange. We are working to make our framework open-source, as we believe that it can serve as a useful source of realistic synthetic data for researchers aiming to study other applications of learning to the domain of kidney exchange.

4.1 Pool Generation

Both of our simulators make use of a *pool generator* that simulates the arrival of new vertices into the pool. We model the arrival of vertices in the pool by letting each patient-donor pair have features independently and identically distributed by some joint distribution f_P on the feature space \mathcal{F} . Each altruist similarly has i.i.d features drawn from a distribution f_A . We let the number of patient-donor pairs and altruists that arrive each iteration be Poisson distributed with arrival rates λ_P and λ_A . We justify this assumption in Figure 4 in Appendix C.

The Organ Procurement and Transplantation Network (OPTN) Kidney Paired Donation Datasets for Researchers contains the running match record for the OPTN Kidney Paired Donation Pilot Program run by the United Network for Organ Sharing. The record contains data from the program’s inception in October 2010 through November 2017. We approximate f_P and f_A by extracting the features of the roughly 3000 patient-donor pairs and altruists. To support computation of the LKDPI metric, we augmented the data by adding extra features – these are outlined in Table 1. Donor/Patient sex and donor/patient weight were drawn jointly using statistics from [Saidman *et al.*, 2006]. Donor eGFR was computed using the well-known MDRD GFR Equation [Levey *et al.*, 1999] given the donor creatinine, race, and age, which were provided in the OPTN dataset, in conjunction with donor sex, which was generated synthetically. We find that in the OPTN exchange, $\lambda_P \approx 4.77$ and $\lambda_A \approx 0.15$. In our experiments, we modify λ_P to simulate kidney exchanges of different sizes.

4.2 Batch and Trajectory Simulation

We develop two simulators in this paper. The *batch simulator* is the first of these two, and is used to generate match

records that we use as training data. It takes as input the number of days D to simulate, and draws a sample record R_T where $T := \frac{D}{\eta}$ denotes the number of match iterations to run, and η denotes the match frequency. In the OPTN exchange, $\eta \approx 5.8$. The trajectory simulator is used to draw samples from the test distribution, and takes as input the compatibility graph $G(T)$ after batch simulation. It samples S vertices v_1^*, \dots, v_S^* from the pool generator, and draws τ values from the distribution of the outcomes $O(v_i^*), W(v_i^*), Q(v_i^*)$ given that $v_i^* \in A(T+1)$. We implement the trajectory simulator by making τS parallel calls to the `SampleSimulator` algorithm, which draws a single match outcome given the features of the sample. Both of our simulators make use of a fairly complex core subroutine `StepPool` which takes as input the pool generator and the current state of the pool $G(t)$, and steps the pool forward by one iteration. The pseudo-code for each of these algorithms in addition to other simulation details can be found in Appendix C.

5 Distributional Shift and Steady-State Kidney Exchanges

D	REC_A	REC_B	DON_A	DON_B
1000	0.32	0.21	0.78	0.54
50000	0.22	0.15	0.78	0.48
Test	0.24	0.17	0.79	0.50

Table 2: **Observed Distributional Shift.** The average values of four features used for prediction from the simulated match record of a pool that is (i) 1000 days old (ii) 50000 days old, and (iii) the test distribution.

In this section, we look more closely at the distributional shift in our learning task. Recall that although we aim to predict outcomes $O(v)$, $W(v)$, and $Q(v)$ for a vertex $v \in A(T+1)$ that has just arrived, we only have as data the outcomes of vertices $u \in \mathcal{R}_T = \bigcup_{t=1}^T D(t)$ of vertices that have exited the pool. As the matching mechanism may tend to match certain types of vertices over others, these distributions are not equal. However, in Table 2 we observe an interesting phenomenon where the distributional shift seemingly disappears in kidney exchanges that have been running for a long time. This is not simply a consequence of having a better estimate for the average due to more training data (i.e., that $|\mathcal{R}_{T_1}| > |\mathcal{R}_{T_0}|$ if $T_1 > T_0$); we control for differences in the sizes of the match records by aggregating many match records for the pool of age 1000 so that both empirical distributions have the same sample size of roughly 6000. We give a strong theoretical justification for why this shift disappears in terms of the steady-state behavior of kidney exchanges.

5.1 Steady-State Exchanges

Although only a few theoretical results exist in simplified models [Toulis and Parkes, 2015; Anderson *et al.*, 2017], it is well-known that many fielded exchanges are in *steady-state* – that is, the number of arrivals is roughly the number of departures $|A(T)| \approx |D(T)|$. We define the steady-state parameter

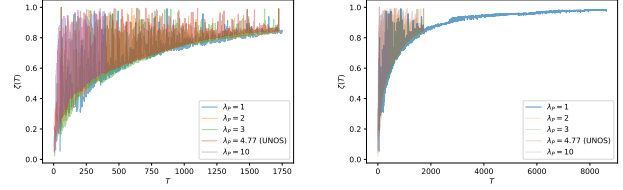


Figure 1: **Kidney Exchanges Approaching Steady-State.** On the left, we plot the steady-state parameter $\zeta(T)$ for simulated kidney exchanges of varying size for 10,000 days. On the right, we extend the plot for the smallest exchange (for computational reasons) to 50,000 days.

at iteration T as

$$\zeta(T) := \frac{\left| \bigcup_{t=1}^T D(t) \right|}{\left| \bigcup_{t=1}^T A(t) \right|} = \frac{\sum_{t=1}^T |D(t)|}{\sum_{t=1}^T |A(t)|} \quad (1)$$

For simplicity, we define $A_T := \sum_{t=1}^T |A(t)|$ and $D_T := \sum_{t=1}^T |D(t)|$. Note that $\zeta(T) \in [0, 1]$. A kidney exchange in steady-state should have $\zeta(T) \approx 1$, as the total number of departures should approach the total number of arrivals. Although extremely intractable to study analytically, Figure 1 shows that the stochastic function $\zeta(T)$ follows a highly well-behaved lower-bound, no matter the size of exchange. Interestingly, as shown in the right plot of Figure 1, $\zeta(T)$ suddenly appears to become much-less noisy after it passes the inflection point of this lower bound.

5.2 Relating Distributional Shift to the Steady-State Parameter

We now show how the distributional shift can be bounded in terms of $\zeta(T)$. Let $\mathcal{R}_T = \{\mathbf{u}_1, \dots, \mathbf{u}_{D_T}\}$ be the set of vertices in the match record. We further have that $\mathcal{R}_T \subseteq \bigcup_{t=1}^T A(t) := \{\mathbf{v}_1, \dots, \mathbf{v}_{A_T}\}$. To make the analysis tractable, we assume that the feature space $\mathcal{F} = \mathbb{R}^d$ is continuous, and that the distribution over the features of any arrival $\mathbf{v}_i \sim f_P = \mathcal{N}(\boldsymbol{\mu}, \Sigma)$ are jointly Gaussian with mean $\boldsymbol{\mu}$ and full-rank covariance Σ . We measure the distributional shift by considering *shifted directions* – directions in which the training data differs statistically from the test distribution. Formally, we say that a unit vector $\mathbf{z} \in \mathbb{R}^d$ is δ -shifted if

$$\sup_{x \in \mathbb{R}} \left| \frac{1}{D_T} \sum_{i=1}^{D_T} \mathbb{1}[\mathbf{z}^T (\mathbf{u}_i - \boldsymbol{\mu}) \leq x] - \Phi\left(\frac{x}{\sqrt{\mathbf{z}^T \Sigma \mathbf{z}}}\right) \right| > \delta \quad (2)$$

Here Φ refers to the CDF of a standard normal variable. This definition basically requires that the Kolmogorov distance between the empirical CDF of the projected data from the match record and the true CDF of the projected arrivals exceeds δ . We say that \mathcal{R}_T is (γ, δ) -shifted if there is a set of δ -shifted directions that have uniform measure γ (or in other words, $\Pr_{\mathbf{z} \sim \mathcal{N}(\mathbf{0}, I)} \left[\frac{\mathbf{z}}{\|\mathbf{z}\|_2} \text{ is } \delta\text{-shifted} \right] > \gamma$). We show that when $\zeta(T) \approx 1$, \mathcal{R}_T is not (γ, δ) -shifted with high probability – that is, if the kidney exchange is at steady-state, the

match record cannot be shifted in too many directions. As $\mathcal{R}_T \subseteq \bigcup_{t=1}^T A(t)$ is a (perhaps even adversarially/arbitrarily chosen) subset of the arrivals, its entries are not distributed as $\mathcal{N}(\boldsymbol{\mu}, \Sigma)$. We can, however, upper bound the probability that \mathcal{R}_T is (γ, δ) -shifted by taking the union bound over all fixed coalitions of size D_T in $\bigcup_{t=1}^T A(t)$. If $\zeta(T)$ is large, then there cannot be too many of these coalitions. This simplification is useful, as the features of any fixed coalition of vertices in $\bigcup_{t=1}^T A(t)$ are normally distributed as $\mathcal{N}(\boldsymbol{\mu}, \Sigma)$.

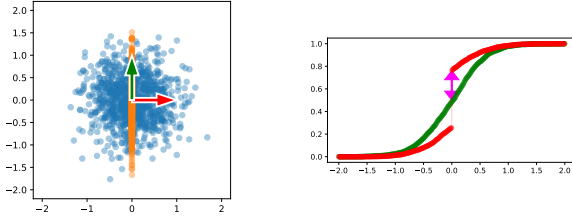


Figure 2: **Shifted Directions.** On the left, we consider a multivariate isotropic Gaussian (in blue) that has been shifted by mixing the distribution with a one-dimensional Gaussian (in orange). On the right, we plot the empirical CDFs given by projecting the data onto the green and red directions. The data remains unshifted in the green direction, but is 0.2615-shifted in the red direction, as shown in magenta.

Using standard tools from empirical process theory (namely the DKWM inequality, restated as Lemma D.1), we show using a probabilistic approach that \mathcal{R}_T is a (γ, δ) -shifted with low probability:

Theorem 5.1. *Let $\mathcal{R}_T = \bigcup_{t=1}^T D(t)$ denote the match record at time T , and let any vertex $v_i \in \bigcup_{t=1}^T A(t)$ have features that are normally distributed as $\mathcal{N}(\boldsymbol{\mu}, \Sigma)$ where Σ is full rank. Then,*

$$\Pr[\mathcal{R}_T \text{ is } (\gamma, \delta)\text{-shifted}] \leq \underbrace{\left(\frac{e}{1-\zeta(T)}\right)^{A_T(1-\zeta(T))}}_{\text{Number of coalitions}} \underbrace{2^{\lceil \gamma d \rceil} \exp(-2A_T \zeta(T) \lceil \gamma d \rceil \delta^2)}_{\text{Probability that a fixed coalition is shifted}}$$

The full proof of Theorem 5.1 can be found in Appendix D. Figure 3 shows how our bounds vary with $\zeta(T)$, A_T , and d . If the feature space is lower dimensional (e.g., $d \approx 10$), we find that our bound produces trivial results when $\zeta(T) \lesssim 0.8$. Immediately after this threshold, however, the probability that the match record is shifted becomes astronomically small. Interestingly, as the dimensionality d of the feature space increases, the well-known ‘‘curse of dimensionality’’ in fact *behaves as a blessing*. High dimensional space contains many directions, and it is difficult for an adversary to shift the distribution in a constant fraction of these at once. This is reflected in our bound, as we see that the probability decreases exponentially in d . We visualize this phenomenon in Figure 3 – even small exchanges (corresponding to a small value for A_T) that are not in steady-state (i.e., $\zeta(T) \approx 0$) remain unshifted when the dimension d exceeds 30.

In practice, many fielded exchanges have been observed to be at or near steady-state [Biró *et al.*, 2019], and matching

policies tend to make use of at least 20–30 features [OPTN, 2021]. However, as demonstrated in Section 7, only 10–20 are highly relevant for prediction. Thus, we obtain some benefits from the dimensionality, but perhaps not enough to eliminate the distributional shift in kidney exchanges far from steady-state.

6 Experiments

We now evaluate our random forest approach on simulated match data. For varying arrival rates λ_P corresponding to kidney exchanges of different sizes, we use the batch simulator described in Section 4.2 to generate simulated match records \mathcal{R}_T . We generate test data for each of these pools by running the trajectory simulator with $S = 300$ samples and $\tau = 500$ trajectories. Trajectory simulation is very computationally intensive, taking about a week to terminate on an HPC cluster. We set $T = 259$, which corresponds to $D = 1500$ days (or roughly 4 years), to prevent pool sizes for the larger exchanges we tested from becoming too large. We also tested our two smallest exchanges setting $D = 4000$ days (or roughly 11 years), and our smallest exchange setting $D = 50000$ days (or roughly 136 years) to understand the performance of our approach on older kidney exchanges. The OPTN exchange is now 11 years old, so our experiments for $D = 4000$ (in addition to those for $D = 1500$) do correspond to benchmarks for realistic exchanges. With the exception of the $D = 50000$ experiment, we re-run all experiments in a federated learning setting where 5 exchanges of the same age aggregate their match records together for prediction. When we aggregate the match records of similar exchanges together, we increase the size of the training dataset while keeping the steady state parameter ζ (and thus the distributional shift) roughly the same. Thus, these experiments allow us to understand whether poor performance is due to insufficient data or distributional shift.

As described in Section 3, we use a random forest classifier to predict the outcome $O(v)$, and we use quantile regression forests to produce 95% prediction intervals for the waiting time $W(v)$ and quality $Q(v)$ conditioned on a match. Letting v_1^*, \dots, v_S^* denote the S samples drawn by the trajectory simulator, we evaluate our classifier by computing the mean absolute error $\text{MAE}(\hat{O}) := \frac{1}{S} \sum_{i=1}^S \left| \hat{O}(v_i^*) - \Pr[O(v_i^*) = 1] \right|$. We evaluate the prediction intervals \widehat{W}_{95} and \widehat{Q}_{95} using the mean *intersection over union* (IOU), which computes the length of the intersection of the intervals divided by the length of the union of the intervals $\text{IOU}(\widehat{W}_{95}) = \frac{1}{S} \sum_{i=1}^S \frac{|\widehat{W}_{95}(v_i^*) \cap W_{95}(v_i^*)|}{|\widehat{W}_{95}(v_i^*) \cup W_{95}(v_i^*)|}$. We estimate the true parameters $\Pr[O(v_i^*) = 1]$, $W_{95}(v_i^*)$, and $Q_{95}(v_i^*)$ from the τ sampled trajectories.

Table 3 shows our experimental results. We consider MAE scores less than 0.2 and IOU scores greater than 0.5 as good performance. The classifier performance $\text{MAE}(\hat{O})$ seems to be primarily determined by the dataset size. This is especially evident in the federated setting, where aggregating multiple match records together always improved performance by as much as 7.6%. Performance for waiting time prediction, on

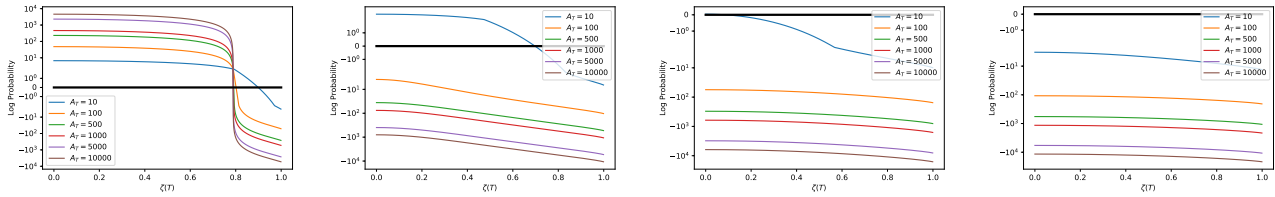


Figure 3: **Steady-State Exchanges are Unshifted.** We plot the log of our bound from Theorem 5.1 on a log scale as $\zeta(T)$ varies from 0 to 1 for six values of A_T , fixing $\gamma = \delta = 0.3$. From left to right, we vary the dimension d from 10 to 40 in increments of 10. We plot in black the trivial upper bound of 1 on the probability to show when our bounds produce nontrivial results.

Arrival Rate	D	Federated	$ R_T $	ζ	MAE (\hat{O})	IOU (\hat{W}_{95})	IOU (\hat{Q}_{95})
$\lambda_P = 1$	1500	No	56	0.397	0.258	0.451	0.747
$\lambda_P = 1$	4000	No	246	0.953	0.191	0.644	0.761
$\lambda_P = 1$	50000	No	4888	0.984	0.130	0.653	0.632
$\lambda_P = 2$	1500	No	157	0.477	0.221	0.336	0.815
$\lambda_P = 2$	4000	No	752	0.882	0.212	0.620	0.809
$\lambda_P = 3$	1500	No	285	0.523	0.184	0.386	0.798
$\lambda_P \approx 4.77$ (OPTN)	1500	No	593	0.509	0.164	0.503	0.812
$\lambda_P = 1$	1500	Yes	268	0.457	0.246*	0.232	0.816*
$\lambda_P = 1$	4000	Yes	1224	0.891	0.148*	0.590	0.800*
$\lambda_P = 2$	1500	Yes	807	0.550	0.145*	0.373*	0.816*
$\lambda_P = 2$	4000	Yes	3773	0.872	0.119*	0.775*	0.820*
$\lambda_P = 3$	1500	Yes	1434	0.488	0.115*	0.421*	0.815*
$\lambda_P \approx 4.77$ (OPTN)	1500	Yes	2652	0.537	0.103*	0.449	0.812

Table 3: **Experimental Results.** We bold steady-state parameters $\zeta > 0.8$, MAE scores < 0.2 , and IOU scores > 0.5 . We asterisk any federated learning experiments that improve relative performance.

the other hand, appears to be highly dependent on the steady-state parameter. The IOU scores for waiting time can roughly be sorted by ζ , and do not necessarily increase in the federated setting, indicating that distributional shift is likely affecting the result. Predicting the organ quality appears to be an easy task – every experiment produced good performance, well exceeding our benchmark IOU of 0.5. This is especially impressive, as the smallest exchange we tested had a match record with only 56 entries. Federated learning improved scores in all cases but one.

Overall, our experiments demonstrate that kidney exchanges of any size that are roughly 4000 days or older may use existing match records to make clinically promising estimates for $O(v)$, $W(v)$, and $Q(v)$. Young exchanges that are relatively large may not be able to produce good estimates for waiting time, but can still estimate $O(v)$ and $Q(v)$ reliably well. Young exchanges that are also small likely cannot estimate the match outcome $O(v)$ or the waiting time $W(v)$, but can still provide patients with good estimates for the organ quality $Q(v)$. Although highly exploratory in nature, our experiments also suggest that federated learning can improve performance – especially when predicting $O(v)$.

7 Diagnosing Mechanism Behavior with SHAP Analysis

In Sections 5 and 6, we demonstrated how, at least for relatively older exchanges, it is possible to train random forest models to produce good estimates for the match outcomes $O(v)$, $W(v)$, and $Q(v)$. These models may serve as decision-support tools to help patients and healthcare workers with medical and insurance decisions. We show how the utility of these models extends beyond this domain – using Shap-

ley additive explanations (SHAP) to compute feature importances [Lundberg and Lee, 2017; Lundberg *et al.*, 2018], in addition to t -Distributed Stochastic Neighbor Embeddings (t -SNE) [Van der Maaten and Hinton, 2008] for visualization, we can use these models to help kidney exchange policy-makers understand how the underlying matching mechanism treats different groups of patients. In Appendix 7, we give background on these techniques, an in-depth explanation of our approach, and a demonstration of its use (and our findings). Although we perform this analysis using data from our simulated OPTN exchange, we emphasize that these techniques may be readily applied to any fielded exchange as our approach only makes use of data from existing match records.

8 Discussion

We proposed and validated a random forest approach to forecast patient outcomes in kidney exchange. We provide strong theoretical and experimental evidence in a state-of-the-art kidney exchange simulation framework that the match outcome $O(v)$, the waiting time $W(v)$, and the organ quality $Q(v)$ can be reliably estimated in older fielded exchanges of any size. Further, $W(v)$ can be estimated well in larger young exchanges, and $Q(v)$ can be estimated well even in smaller young exchanges. As our approach exclusively makes use of existing match records, it may be readily deployed as a decision-support tool in exchanges across the world. Our tool doubles as a principled method for detecting bias and policy miscalibration, and may be used to inform kidney exchange policy; we view this as one step towards increased agency and transparency in kidney exchange.

Acknowledgements

Srinivasan was supported in part by NSF Award CCF-1749864, and by research awards from Adobe, Inc., Amazon, Inc., and Google Inc. Dickerson was supported in part by NSF CAREER Award 184623.

References

- [Agarwal *et al.*, 2019] Nikhil Agarwal, Itai Ashlagi, Eduardo Azevedo, Clayton R Featherstone, and Ömer Karaduman. Market failure in kidney exchange. *American Economic Review*, 109(11):4026–70, 2019.
- [Anderson *et al.*, 2017] Ross Anderson, Itai Ashlagi, David Gamarnik, and Yash Kanoria. Efficient dynamic barter exchange. *Operations Research*, 65(6):1446–1459, 2017.

- [Ashlagi and Roth, 2014] Itai Ashlagi and Alvin E Roth. Free riding and participation in large scale, multi-hospital kidney exchange. *Theoretical Economics*, 9(3):817–863, 2014.
- [Ashlagi and Roth, 2021] Itai Ashlagi and Alvin Roth. Kidney exchange: an operations perspective. *Management Science*, 2021.
- [Biró *et al.*, 2019] Péter Biró, Bernadette Haase-Kromwijk, Tommy Andersson, Eyjólfur Ingi Ásgeirsson, Tatiana Balesová, Ioannis Boletis, Catarina Bolotinha, Gregor Bond, Georg Böhmig, Lisa Burnapp, et al. Building kidney exchange programmes in europe—an overview of exchange practice and activities. *Transplantation*, 103(7):1514, 2019.
- [Cox, 1992] David R Cox. Regression models and life-tables. In *Breakthroughs in Statistics*, pages 527–541. Springer, 1992.
- [Dickerson and Sandholm, 2015] John P. Dickerson and Tuomas Sandholm. FutureMatch: Combining human value judgments and machine learning to match in dynamic environments. In *AAAI Conference on Artificial Intelligence (AAAI)*, pages 622–628, 2015.
- [Dickerson *et al.*, 2014] John P. Dickerson, Ariel D. Procaccia, and Tuomas Sandholm. Price of fairness in kidney exchange. In *International Conference on Autonomous Agents and Multi-Agent Systems (AAMAS)*, pages 1013–1020, 2014.
- [Hinton and Roweis, 2002] Geoffrey Hinton and Sam T Roweis. Stochastic neighbor embedding. In *Conference on Neural Information Processing Systems (NeurIPS)*, volume 15, pages 833–840. Citeseer, 2002.
- [Levey *et al.*, 1999] Andrew S Levey, Juan P Bosch, Julia Breyer Lewis, Tom Greene, Nancy Rogers, and David Roth. A more accurate method to estimate glomerular filtration rate from serum creatinine: a new prediction equation. *Annals of internal medicine*, 130(6):461–470, 1999.
- [Lundberg and Lee, 2017] Scott Lundberg and Su-In Lee. A unified approach to interpreting model predictions. In *Conference on Neural Information Processing Systems (NeurIPS)*, 2017.
- [Lundberg *et al.*, 2018] Scott M Lundberg, Gabriel G Erion, and Su-In Lee. Consistent individualized feature attribution for tree ensembles. *arXiv preprint arXiv:1802.03888*, 2018.
- [Lundberg *et al.*, 2020] Scott M Lundberg, Gabriel Erion, Hugh Chen, Alex DeGrave, Jordan M Prutkin, Bala Nair, Ronit Katz, Jonathan Himmelfarb, Nisha Bansal, and Su-In Lee. From local explanations to global understanding with explainable AI for trees. *Nature machine intelligence*, 2(1):56–67, 2020.
- [Massart, 1990] Pascal Massart. The tight constant in the Dvoretzky-Kiefer-Wolfowitz inequality. *The Annals of Probability*, pages 1269–1283, 1990.
- [Massie *et al.*, 2016] Allan B Massie, Joseph Leanza, LM Fahmy, EKH Chow, Niraj M Desai, X Luo, EA King, MG Bowring, and DL Segev. A risk index for living donor kidney transplantation. *American Journal of Transplantation*, 16(7):2077–2084, 2016.
- [Meinshausen and Ridgeway, 2006] Nicolai Meinshausen and Greg Ridgeway. Quantile regression forests. *Journal of Machine Learning Research*, 7(6), 2006.
- [Neuen *et al.*, 2013] Brendon L Neuen, Georgina E Taylor, Alessandro R Demaio, and Vlado Perkovic. Global kidney disease. *The Lancet*, 382(9900):1243, 2013.
- [OPTN, 2021] OPTN. Organ Procurement and Transplantation Network (OPTN) policies, 2021. Policy 13: Kidney Paired Donation (KPD). Available online: https://optn.transplant.hrsa.gov/media/1200/optn_policies.pdf.
- [Rao *et al.*, 2009] Panduranga S Rao, Douglas E Schaubel, Mary K Guidinger, Kenneth A Andreoni, Robert A Wolfe, Robert M Merion, Friedrich K Port, and Randall S Sung. A comprehensive risk quantification score for deceased donor kidneys: the kidney donor risk index. *Transplantation*, 88(2):231–236, 2009.
- [Roth *et al.*, 2004] Alvin Roth, Tayfun Sönmez, and Utku Ünver. Kidney exchange. *Quarterly Journal of Economics*, 119(2):457–488, 2004.
- [Roth *et al.*, 2005a] Alvin Roth, Tayfun Sönmez, and Utku Ünver. A kidney exchange clearinghouse in New England. *American Economic Review*, 95(2):376–380, 2005.
- [Roth *et al.*, 2005b] Alvin Roth, Tayfun Sönmez, and Utku Ünver. Pairwise kidney exchange. *Journal of Economic Theory*, 125(2):151–188, 2005.
- [Saidman *et al.*, 2006] Susan L. Saidman, Alvin Roth, Tayfun Sönmez, Utku Ünver, and Frank Delmonico. Increasing the opportunity of live kidney donation by matching for two and three way exchanges. *Transplantation*, 81(5):773–782, 2006.
- [Santos *et al.*, 2015] Alfonso H Santos, Michael J Casey, Xuerong Wen, Ivan Zendejas, Shehzad Rehman, Karl L Womer, and Kenneth A Andreoni. Survival with dialysis versus kidney transplantation in adult hemolytic uremic syndrome patients: A fifteen-year study of the waiting list. *Transplantation*, 99(12):2608–2616, 2015.
- [Sönmez *et al.*, 2017] Tayfun Sönmez, Utku Ünver, and M Bumin Yenmez. Incentivized kidney exchange, 2017. Tech. report, Boston College Dept. of Economics.
- [Toulis and Parkes, 2015] Panos Toulis and David C. Parkes. Design and analysis of multi-hospital kidney exchange mechanisms using random graphs. *Games and Economic Behavior*, 91(0):360–382, 2015.
- [UNOS, 2015] UNOS. Revising kidney paired donation pilot program priority points, 2015. OPTN/UNOS Public Comment Proposal.
- [Van der Maaten and Hinton, 2008] Laurens Van der Maaten and Geoffrey Hinton. Visualizing data using *t*-SNE. *Journal of Machine Learning Research*, 9(11), 2008.

Supplementary Material for Submission 12935

A Additional Information about Kidney Exchange

A.1 Deceased- & Living-Donor Kidney Allocation

Our motivation in this paper is, in part, due to the widespread usage of the Kidney Donor Profile Index (KDPI) to quantify the value of deceased-donor kidneys, and the increasing use of the newer Living Kidney Donor Profile Index (LKDPI) to quantify the value of living-donor kidneys [Rao *et al.*, 2009; Massie *et al.*, 2016]. Roughly speaking, both the KDPI and the LKDPI are metrics used to compute the expected lifetime (quality) of a kidney that is donated from a donor D to a patient P . Both are based on multivariate Cox Regression models adapted from the traditional statistics literature [Cox, 1992]. The LKDPI metric was constructed such that LKDPI scores can be directly compared with KDPI scores, thus allowing direct comparison between living donor and deceased donor options. We expand this metric of quality to fielded kidney exchange by computing a 95% prediction interval for the LKDPI of the kidney received through kidney-paired donation. Thus, our system provides patients with the ability to make an informed comparison between the living donor, deceased donor, and kidney-paired donation options. Because we build on the LKDPI metric in this paper, we formally restate its calculation below.

$$\begin{aligned} \text{LKDPI}(D, P) = & - 11.30 \\ & + 1.85 * [(D_{\text{age}} - 50) \text{ if } D_{\text{age}} > 50] \\ & - 0.381 * D_{\text{eGFR}} \\ & + 1.17 * D_{\text{BMI}} \\ & \quad (+22.34 \text{ if } D_{\text{is African-American}}) \\ & \quad (+14.33 \text{ if } D_{\text{has history of cigarette use}}) \\ & + 0.44 * D_{\text{systolic blood pressure}} \\ & \quad (-21.68 \text{ if } D \text{ and } P \text{ are both male}) \\ & \quad (+27.30 \text{ if } D \text{ and } P \text{ are ABO incompatible}) \\ & \quad (-10.61 \text{ if } D \text{ and } P \text{ are unrelated}) \\ & + 8.57 * (\# \text{HLA-B mismatches}) \\ & + 8.26 * (\# \text{HLA-DR mismatches}) \\ & - 50.87 * \left[\min \left(\frac{D_{\text{weight}}}{P_{\text{weight}}}, 0.9 \right) \right] \end{aligned}$$

Here, the estimated glomerular filtration rate (eGFR), body mass index (BMI), blood type (ABO) compatibility, and human leukocyte antigen (HLA) are all integral or real values determined by physical medical testing.²

A.2 The Kidney Exchange Integer Program

Recall from Section 2 that we aim to compute $M^*(T) \in \arg \max_{M \in \mathcal{M}(T)} u(M)$, where $u(M)$ denotes the utility of some match $M \in \mathcal{M}(T)$. Finding a maximum weight (capped-length) cycle and chain packing is NP-hard, and is also hard to approximate. In practice, integer program (IP) formulations are used to clear large exchanges. Formally, let the legal matchings $\mathcal{M}(T) = \mathcal{C}_{G(T)}(L, K)$ be given by the set of all legal chains of length at most K and cycles of length at most L . Then, solve the IP: $\max \sum_{c \in \mathcal{C}_{G(T)}(L, K)} w_c x_c$ subject to $\sum_{c: v \in c} x_c \leq 1 \quad \forall v \in V(T)$, where $x_c \in \{0, 1\}$ is a variable for every $c \in \mathcal{C}_{G(T)}(L, K)$, and $w_c = \sum_{(v_i, v_j) \in c} w(v_i, v_j)$. The final matching is the set of chains and cycles c such that $x_c = 1$. We use this IP as a sub-solver – an open-source implementation can be found at <https://github.com/JohnDickerson/KidneyExchange>. For a comprehensive overview of operations-research-based kidney exchange clearing techniques, we direct the reader to a recent survey by Ashlagi and Roth [Ashlagi and Roth, 2021].

²While we direct the reader to the medical literature for a full explanation of all variables in this equation [Massie *et al.*, 2016], we overview ABO compatibility here. At a high level, blood is partitioned into four types: O, A, B, and AB. Blood type O, known as the “universal donor” type, can be donated to patients of any other blood type. Blood types A and B can be donated to types A and B, respectively, along with type AB; blood type AB can be donated only to those of type AB blood. A donor whose blood type can be donated to a patient is said to be an *ABO compatible* donor.

B Model Details

Categorical Encoding for HLA Features. As described in Table 1, there are two sets of categorical features that we use for prediction: the patient and donor blood types, and the patient and donor human leukocyte antigen (HLA) vectors. Although each blood type may be sensibly encoded as two Boolean features, as described in Section 3, the HLA vector requires a more involved approach. Formally, the HLA vector consists of three components relevant for matching: the HLA-A vector, the HLA-B vector, and the HLA-DR vector. Each of these vectors contains two components, and each of these components is a categorical variable with between 20 – 40 categories. Thus, naively one-hot encoding the HLA vector leads to an impractical number of additional data dimensions.

To resolve this, we make the observation that in both the LKDPI formula, and the OPTN matching policy [UNOS, 2015], each of these vectors are used exclusively in computing the number of *mismatches* one vertex has relative to the HLA vectors of another vertex. Thus, we encode the vectors based on how common they are in the general population. We may estimate commonality either by considering statistics for an entire national or global population, or, if the match record \mathcal{R}_T is sufficiently large/close to steady-state, we may use statistics from the record itself. We introduce 10 features to encode the three HLA vectors. We first individually compute how common each of the 6 components are of the three vectors. Next, for each of the three HLA vectors, we compute how common each vector is in some sample population using the joint statistics for the components. Finally, we compute how jointly common all three vectors together are.

Training Details. We used the Scikit-Garden framework <https://scikit-garden.github.io/> to implement the quantile regression forest models described in this paper. We set the number of estimators to 1000, and set the minimum number samples to split on an internal node equal to 10. These parameters were selected by grid search, using 25% of the match record \mathcal{R}_T for validation. We found that our models were not, in general, that sensitive to choices of hyperparameters – we observed no meaningful difference in performance using these parameters versus the Scikit-Garden defaults.

C Simulating the Kidney Exchange

C.1 Justifying the Arrival Rate

As discussed in Section 4.1, our simulators make use of a *pool generator* to sample the set of arrivals $A(T)$ at time T ; formally, this consists of distributions f_P and f_A denoting the feature distributions of the patient-donor pairs and altruists respectively, along with parameters λ_P and λ_A that similarly denote the arrival rates of these two types of vertices respectively.

We make the assumption that both the features of any vertex of a given class (patient-donor pair or altruist) are independently and identically distributed by the joint distribution f_P or f_A within the set $A(T)$, and over time T . This holds in practice as the biological features of one vertex cannot affect those of another, and are drawn from the same (large) population. More complex is the distribution over the number of arrivals $|A(T)|$ – there is no principled reason to believe a priori that this quantity is independently and identically distributed over time. If the expected number of arrivals in the exchange grew nonlinearly, for example, the distribution over $|A(T)|$ *must* change with time. However, we find, using empirical data from the OPTN Dataset for Researchers, that the number of arrivals $|A(T)|$ are indeed i.i.d and approximately Poisson in practice, after a short “warm-up” period. This is shown in Figure 4.

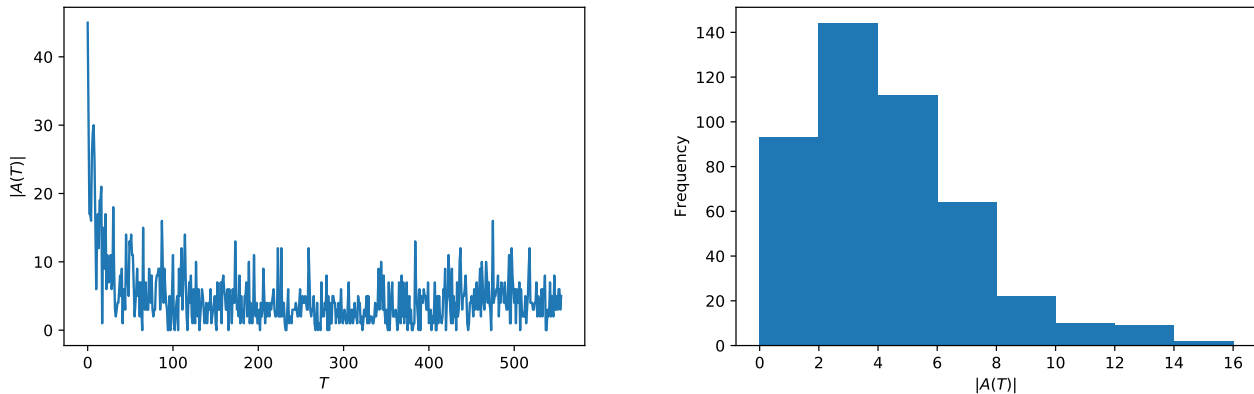


Figure 4: **Arrival Rates in a Fielded Exchange.** On the left, we plot the the number of arrivals each match iteration. On the right, we show the empirical distribution for the number of arrivals, after the initial 100-iteration warm-up period.

C.2 Pseudo-code for Simulation

In this section, we give the pseudo-code for the routines described in Section 4.2. Both of our simulators make use of the core subroutine `StepPool` – we give the pseudo-code for this routine here as well, in addition to a brief description of its various components.

Algorithm 1: `BatchSimulator`

Input: $\lambda_P, \lambda_A, f_P, f_A, T$
Output: $\mathcal{R}_T, G(T)$
 $\mathcal{R}_T, G(0) := \emptyset;$
for $t \in [T]$ **do**
 $G(t), D(t) := \text{StepPool}(\lambda_P, \lambda_A, f_P, f_A, G(t-1));$
 $\mathcal{R}_T := \mathcal{R}_T \cup D(t)$
end
return $\mathcal{R}_T, G(T);$

The batch simulator is the simplest of the routines listed here. It generates simulated match records by simply stepping the pool forward in time until the given time threshold T , aggregating the departure sets $D(t)$ with labeled outcomes into the match record \mathcal{R}_T along the way. The time threshold T is given by dividing the number of days to simulate D by the match frequency η . The outcomes (O, W, Q) are labeled in `StepPool`.

Algorithm 2: SampleSimulator

```
Input:  $\lambda_P, \lambda_A, f_P, f_A, G(T), v^*, \kappa$   
Output: Sample outcomes  $O(v^*), W(v^*), Q(v^*)$   
 $V(T) := V(T) \cup \{v^*\};$  // Add  $v^*$  to the pool  
/* Redraw edges to include the new vertex */  
 $E(T) := \text{ABOCompatible}(V(T));$  // Draw edges between compatible vertices  
for  $(u, v) \in E(T)$  do  
|  $\text{Weight}(u, v) := w_{\text{OPTN}}(u, v);$  // Weight edges with the UNOS Policy [UNOS, 2015]  
end  
for  $t \in [T + 1, \kappa]$  do  
|  $G(t), D(t) := \text{StepPool}(\lambda_P, \lambda_A, f_P, f_A, G(t - 1));$   
| /* Return patient outcomes if  $v^*$  exited the pool */  
| if  $v^* \in D(t)$  then  
| | return  $O(v^*), W(v^*), Q(v^*)$   
| end  
end  
return  $\emptyset, \emptyset, \emptyset;$  // Simulation timed out
```

The trajectory simulator samples τ outcomes of $O(v_i^*), W(v_i^*),$ and $Q(v_i^*)$ for S random vertices v_1^*, \dots, v_S^* with features drawn by f_P by making τS parallel calls to the `SampleSimulator` routine. This algorithm adds a given vertex v^* to the compatibility graph $G(T)$ given at the end of batch simulation, and steps the pool forward until the vertex exits the pool. To prevent hard-to-match vertices from never clearing the pool, we introduce a cutoff parameter $\kappa = 600$ (corresponding to roughly 9.5 years) that caps the length of the simulation.

We now describe the routine `StepPool` which steps a compatibility graph $G(t)$ one iteration forward in time given the pool generator. After initializing the departure set for the next iteration, we first compute an optimal matching $M^*(t)$ using the integer program described in Section A.2. In practice, we compute this IP using an open-source codebase [Dickerson and Sandholm, 2015].

Next, we `Expire` vertices with constant probability based on the fraction of vertices that exit the OPTN exchange each match iteration for any reason other than a successful match. We then iterate through the constituent cycles and vertices in $M^*(t)$ to determine which of these proposed matches are successful. Any cycle is removed if *any* of its constituent edges fail the more comprehensive crossmatch test. The chance of a `NegativeCrossmatch` is given by the patient’s sensitivity, or calculated panel of reactive antibodies (CPRA). A patient with a CPRA of 100, for example, would fail the crossmatch test with probability 1. Chains may similarly fail due to a `NegativeCrossmatch`, and may additionally fail if the next paired-donor in the `Renege` on the promise to continue chain. However, unlike in a cycle, all vertices prior to the vertex at which the chain failed still obtain a successful match.

Finally, we draw the new arrivals from the pool generator, and evolve the vertex set as described in Section 2. To complete the process, we first construct the directed set of edges by drawing an edge between any two vertices where the donor of one vertex has a blood-type that matches the patient of the other. The edges are then weighted using the OPTN point system [UNOS, 2015] to create the final compatibility graph.

Algorithm 3: StepPool

```
Input:  $\lambda_P, \lambda_A, f_P, f_A, G(t)$ 
Output:  $G(t+1), D(t)$ 
 $D(t+1) := \emptyset;$ 
 $M^*(t) := \text{SolveIP}(G(t));$  // Solve the IP from Section A.2
for  $v \in V(t+1)$  do
  if  $\text{Expire}(v)$  then
     $D(t+1) := D(t+1) \cup \{v\};$ 
    /* Remove any matches containing  $v$  from  $M^*(t)$  */
     $M^*(t) := M^*(t) \setminus \{v\};$ 
     $O(v) := 0;$  // Set outcome as not matched
  end
end
for  $c \in \text{Cycles}(M^*(t))$  do
  for  $v \in c$  do
    if  $\text{NegativeCrossmatch}(v)$  then
      /* If the crossmatch test fails, the entire cycle is removed */
       $M^*(t) := M^*(t) \setminus \{c\};$ 
    end
  end
end
for  $c \in \text{Chains}(M^*(t))$  do
  for  $v \in c$  do
    if  $\text{Reneges}(v)$  or  $\text{NegativeCrossmatch}(v)$  then
      /* If the donor of  $v$  reneges, the tail of  $c$  is removed */
       $M^*(t) := M^*(t) \setminus \{\text{Tail}(c, v)\};$ 
    end
  end
end
/* Set waiting time and quality for every matched patient */
for  $(u, v) \in M^*(t)$  do
   $O(v) := 1;$  // Set outcome as matched
   $W(v) := t + 1;$ 
   $Q(v) := \text{LKDPI}(u, v);$  // Compute LKDPI between donor of  $u$  and patient of  $v$ 
end
 $D(t+1) := D(t+1) \cup M^*(t);$ 
 $A(t+1) := \text{Sample}(\lambda_P, \lambda_A, f_P, f_A);$  // Sample new arrivals
 $V(t+1) := V(t) \cup A(t+1) \setminus D(t+1);$  // Evolve the pool
/* Draw directed edges between ABO compatible vertices */
 $E(t+1) := \text{ABOCompatible}(V(t+1));$ 
for  $(u, v) \in E(t+1)$  do
   $\text{Weight}(u, v) := w_{\text{OPTN}}(u, v);$  // Weight edges with the OPTN Policy [UNOS, 2015]
end
 $G(t+1) := (V(t+1), E(t+1));$ 
return  $G(t+1), D(t);$ 
```

D Proofs of Results from Section 5

We restate our main result:

Theorem 5.1. *Let $\mathcal{R}_T = \bigcup_{t=1}^T D(t)$ denote the match record at time T , and let any vertex $v_i \in \bigcup_{t=1}^T A(t)$ have features that are normally distributed as $\mathcal{N}(\boldsymbol{\mu}, \Sigma)$ where Σ is full rank. Then,*

$$\Pr[\mathcal{R}_T \text{ is } (\gamma, \delta)\text{-shifted}] \leq \left(\frac{e}{1 - \zeta(T)} \right)^{A_T(1 - \zeta(T))} 2^{\lceil \gamma d \rceil} \exp(-2A_T \zeta(T) \lceil \gamma d \rceil \delta^2)$$

Proof. In this proof, we make use of the DKWM inequality. For completeness, we restate it below:

Lemma D.1 (DKWM Inequality [Massart, 1990]). *Suppose n samples are drawn i.i.d. from a distribution with cumulative distribution function F . Then, the empirical CDF F_n satisfies*

$$\Pr \left[\sup_{x \in \mathbb{R}} |F_n(x) - F(x)| > \delta \right] \leq 2e^{-2n\delta^2}$$

Recall that a match record \mathcal{R}_T is (γ, δ) -shifted if there exists a region R of the d -dimensional unit ball S^{d-1} of uniform measure γ such that all directions within R are δ -shifted. It follows that we may upper bound the probability of this event by computing the probability that a finite collection $\mathbf{z}_1, \dots, \mathbf{z}_k$ of directions within R are δ -shifted. We show in Lemma D.2 that one can select at least $k = \lceil \gamma d \rceil$ directions \mathbf{z}_i in a way that makes the analysis more tractable. We state and prove this result:

Lemma D.2. *If \mathcal{R}_T is (γ, δ) -shifted, then there exist $\lceil \gamma d \rceil$ δ -shifted unit vectors $\mathbf{z}_1, \dots, \mathbf{z}_{\lceil \gamma d \rceil}$ such that $\mathbf{z}_i^T \Sigma \mathbf{z}_j = 0$ for any $i \neq j \in [\lceil \gamma d \rceil]$.*

Proof. We show existence probabilistically. As Σ is full rank, there exists an orthogonal basis $\Sigma^{-1/2} \mathbf{e}_1, \dots, \Sigma^{-1/2} \mathbf{e}_d$ under the Σ inner product. Further, for any orthogonal matrix $U \in \mathbb{R}^{d \times d}$, the basis $\Sigma^{-1/2} U \mathbf{e}_1, \dots, \Sigma^{-1/2} U \mathbf{e}_d$ is also orthogonal under the Σ inner product. Thus, we may randomly draw Σ -orthogonal bases $\mathbf{z}_1, \dots, \mathbf{z}_d$ by selecting a matrix U from the group of orthogonal matrices $O(d)$ uniformly at random in the sense of the Haar measure. This joint distribution over $\mathbf{z}_1, \dots, \mathbf{z}_d$ has a special property – the marginal distribution for each \mathbf{z}_i is described by the uniform measure over S^{d-1} . We use this to prove the result.

Let $\mathbf{z}_1, \dots, \mathbf{z}_d$ be distributed as above, and for each $i \in [d]$, let S_i be an indicator variable for the event that \mathbf{z}_i is δ -shifted. We have that

$$\mathbb{E} \left[\sum_{i=1}^d S_i \right] = \sum_{i=1}^d \mathbb{E}[S_i] = \sum_{i=1}^d \Pr[\mathbf{z}_i \text{ is } \delta\text{-shifted}] \geq \gamma d$$

where the final inequality follows by the fact that \mathcal{R}_T is (γ, δ) -shifted, and that each \mathbf{z}_i has a marginal distribution described by the uniform distribution. As $\sum_{i=1}^d S_i$ is an integer that must equal or exceed its expectation with positive probability, we must have that $\lceil \gamma d \rceil$ basis elements must be δ -shifted with positive probability, whence the desired result follows. \square

Using Lemma D.2, we may write, for some $\mathbf{z}_1, \dots, \mathbf{z}_{\lceil \gamma d \rceil}$ such that $\mathbf{z}_i \Sigma \mathbf{z}_j = 0$ for $i \neq j$, that

$$\begin{aligned} \Pr[\mathcal{R}_T \text{ is } (\gamma, \delta)\text{-shifted}] &\leq \Pr \left[\bigcap_{i=1}^{\lceil \gamma d \rceil} \mathbf{z}_i \text{ is } \delta\text{-shifted} \right] \\ &= \Pr \left[\bigcap_{i=1}^{\lceil \gamma d \rceil} \sup_{x \in \mathbb{R}} \left| \frac{1}{D_T} \sum_{j=1}^{D_T} \mathbb{1}[\mathbf{z}_i^T (\mathbf{u}_j - \boldsymbol{\mu}) \leq x] - \Phi \left(\frac{x}{\sqrt{\mathbf{z}_i^T \Sigma \mathbf{z}_i}} \right) \right| > \delta \right] \\ &\leq \binom{A_T}{D_T} \Pr \left[\bigcap_{i=1}^{\lceil \gamma d \rceil} \sup_{x \in \mathbb{R}} \left| \frac{1}{D_T} \sum_{j=1}^{D_T} \mathbb{1}[\mathbf{z}_i^T (\mathbf{v}_j - \boldsymbol{\mu}) \leq x] - \Phi \left(\frac{x}{\sqrt{\mathbf{z}_i^T \Sigma \mathbf{z}_i}} \right) \right| > \delta \right] \\ &= \binom{A_T}{D_T} \prod_{i=1}^{\lceil \gamma d \rceil} \Pr \left[\sup_{x \in \mathbb{R}} \left| \frac{1}{D_T} \sum_{j=1}^{D_T} \mathbb{1}[\mathbf{z}_i^T (\mathbf{v}_j - \boldsymbol{\mu}) \leq x] - \Phi \left(\frac{x}{\sqrt{\mathbf{z}_i^T \Sigma \mathbf{z}_i}} \right) \right| > \delta \right] \end{aligned}$$

In the third line we use that $D_T = \{\mathbf{u}_1, \dots, \mathbf{u}_{D_T}\}$ is a subset of $\bigcup_{t=1}^T A(t) = \{\mathbf{v}_1, \dots, \mathbf{v}_{A_T}\}$ of size D_T , whence we may apply the union bound over subsets $\bigcup_{t=1}^T A(t)$ of size D_T . In the fourth line, we use the fact that the $A_T \cdot D_T$ random variables $\mathbf{z}_i^T (\mathbf{v}_j - \boldsymbol{\mu})$ are independent. To see this, observe that as each of the \mathbf{v}_i are independently and identically distributed

as $\mathcal{N}(\boldsymbol{\mu}, \Sigma)$, $\mathbf{z}_i^T(\mathbf{v}_k - \boldsymbol{\mu})$ is independent from $\mathbf{z}_j^T(\mathbf{v}_l - \boldsymbol{\mu})$ for any i, j and $k \neq l$. Next, noting that these variables are jointly Gaussian, we have that $\mathbf{z}_i^T(\mathbf{v}_k - \boldsymbol{\mu})$ and $\mathbf{z}_j^T(\mathbf{v}_k - \boldsymbol{\mu})$ for any $i \neq j$ and k satisfy

$$\text{Cov}[\mathbf{z}_i^T(\mathbf{v}_k - \boldsymbol{\mu}), \mathbf{z}_j^T(\mathbf{v}_k - \boldsymbol{\mu})] = \mathbf{z}_i^T \mathbb{E}[(\mathbf{v}_k - \boldsymbol{\mu})(\mathbf{v}_k - \boldsymbol{\mu})^T] \mathbf{z}_j = \mathbf{z}_i \Sigma \mathbf{z}_j = 0$$

whence these variables are also independent. Further, observe that $\mathbf{z}_i^T(\mathbf{v}_k - \boldsymbol{\mu}) \sim \mathcal{N}(0, \mathbf{z}_i^T \Sigma \mathbf{z}_i)$, whence the variable has a CDF given by $F^i(x) := \Phi\left(\frac{x}{\sqrt{\mathbf{z}_i^T \Sigma \mathbf{z}_i}}\right)$. Applying the DKWM inequality (Lemma D.1), we find that

$$\begin{aligned} \Pr[\mathcal{R}_T \text{ is } (\gamma, \delta)\text{-shifted}] &\leq \binom{A_T}{D_T} \prod_{i=1}^{\lceil \gamma d \rceil} \Pr\left[\sup_{x \in \mathbb{R}} \left| \frac{1}{D_T} \sum_{j=1}^{D_T} \mathbf{1}[\mathbf{z}_i^T(\mathbf{v}_j - \boldsymbol{\mu}) \leq x] - \Phi\left(\frac{x}{\sqrt{\mathbf{z}_i^T \Sigma \mathbf{z}_i}}\right) \right| > \delta\right] \\ &= \binom{A_T}{D_T} \prod_{i=1}^{\lceil \gamma d \rceil} \Pr\left[\sup_{x \in \mathbb{R}} |F_{D_T}^i - F^i| > \delta\right] \\ &\leq \binom{A_T}{D_T} \prod_{i=1}^{\lceil \gamma d \rceil} 2e^{-2D_T \delta^2} \\ &\leq \left(\frac{eA_T}{A_T - D_T}\right)^{A_T - D_T} 2^{\lceil \gamma d \rceil} \exp(-2D_T \lceil \gamma d \rceil \delta^2) \\ &= \left(\frac{e}{1 - \zeta(T)}\right)^{A_T(1 - \zeta(T))} 2^{\lceil \gamma d \rceil} \exp(-2A_T \zeta(T) \lceil \gamma d \rceil \delta^2) \end{aligned}$$

as desired. Notably, observe that $\left(\frac{e}{1 - \zeta(T)}\right)^{A_T(1 - \zeta(T))}$ bounds the number of coalitions, and $2^{\lceil \gamma d \rceil} \exp(-2A_T \zeta(T) \lceil \gamma d \rceil \delta^2)$ bounds the probability that any coalition gives a (γ, δ) -shifted match record. \square

E Additional Background and Figures from Section 7

E.1 Shapley Additive Explanations and t -SNE

SHAP. We use Shapley Additive Explanations (SHAP) to explore the importance of features in our ML models [Lundberg and Lee, 2017; Lundberg *et al.*, 2018]. SHAP is a local explainability method that has gained prominence in recent years due to its strong theoretical grounding in the cooperative game theory literature; specifically, it is an adaptation of the well-known concept of the Shapley value to the explainable ML setting. While computing Shapley values exactly is NP-hard in the general case, faster methods can be used for special cases. For example, for tree-based ML models such as random forests (like we use in the present work), it is possible to compute Shapley values (and thus run the SHAP explainer) in polynomial time [Lundberg *et al.*, 2020]. We use that fast and exact method in our work.

t -SNE. In Section 7, we make use of the t -distributed stochastic neighbor embedding (t -SNE) to project our relatively high-dimensional input data, consisting of the SHAP values for 29 features, into a lower-dimensional space [Van der Maaten and Hinton, 2008; Hinton and Roweis, 2002]. (Figure 8 below visualizes these raw SHAP values for the top 20 features.) t -SNE is a nonlinear dimensionality reduction technique that places points in a typically two- or three-dimensional space such that, for a given point, similar points are nearby and dissimilar points are not nearby. While the “clusters” that appear in a t -SNE representation of data may not be meaningful in all cases due to t -SNE not maintaining relative distances in its embeddings, it is nonetheless a popular method for exploratory data analysis and visualization of high-dimensional data.

E.2 Overview of Approach and Findings on Simulated Data

We now show how our approach can be used to diagnose the behavior of our simulated OPTN exchange. Figure 5 shows the SHAP summary plots for our random forests that predict $O(v)$, $W(v)$, and $Q(v)$ respectively – indeed, these plots already provide some baseline transparency into the mechanism’s function.

Next, we use t -SNE to project the SHAP values onto 2-dimensional space. These plots are shown in Figure 7. Observe that several well-defined clusters appear upon projection. Points within the same cluster have similar SHAP values, which means that they have similar outputs due to the same underlying explanation. Each cluster in the t -SNE plot for $O(v)$, for example, consists of patients whose biological features contribute similarly in determining whether or not the patient is matched. Thus, at a high level, patient outcomes are determined by assigning the patient to some *explanatory class* characterized by a given cluster. The class decompositions for $Q(v)$ and $W(v)$ are fairly simple, and can be found in Figures 7 and 8 respectively.

As described in Section 2, fielded exchanges explicitly add prioritization for harder-to-match patients through the edge-weighting function w . It is standard (e.g. in the OPTN policy [UNOS, 2015]) for these functions to take the form of a point system where each feature is individually assessed, and assigned a point value that aims to balance biological compatibility with ethical considerations for hard-to-match patients. In practice, there is no existing principled method to set these weights – they are mostly determined ad-hoc.

Our model’s explanatory class decomposition can be used to identify miscalibrations in the policy that unfairly benefit or harm certain demographic groups. In Figure 7, we identify two effect groups that get matched with very high probability. We find, in Figure 6, that patients in these groups have among the most difficult-to-match features, and thus receive prioritization from the matching mechanism. Their paired donors, however, are among the easiest to match. As a result, these patients obtain a distinct advantage over other participants. We can see this advantage more explicitly by observing how the SHAP value for patient sensitivity (CPRA) varies with its value, as in Figure 9. These results indicate that the OPTN policy [UNOS, 2015] may be miscalibrated for sensitized patients.

E.3 Referenced Figures

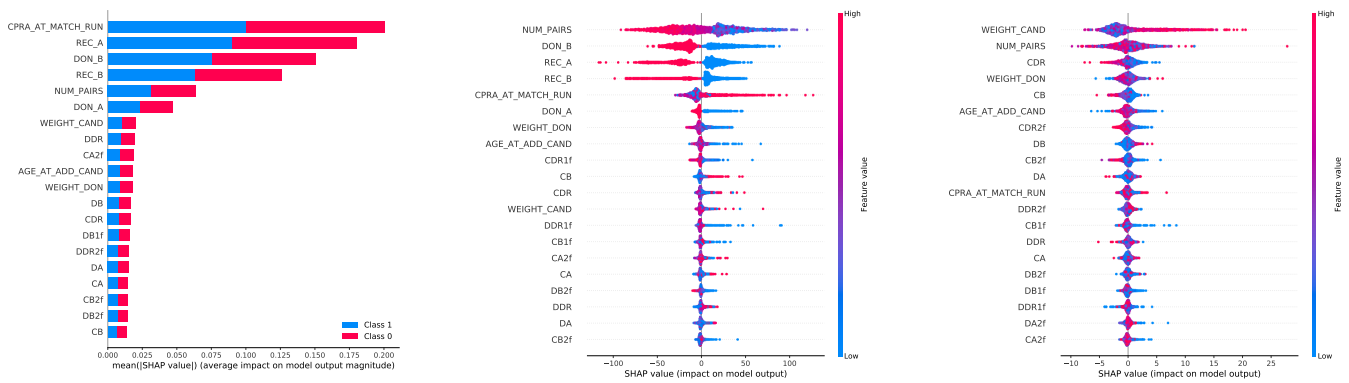


Figure 5: **SHAP Summary Plots.** We plot from left to right the relative feature importances for the top 20 features in predicting the match outcome $O(v)$, the waiting time $W(v)$, and the organ quality $Q(v)$. We find, somewhat unsurprisingly, that the same few features (patient CPRA, REC_A, REC_B, DON_A, DON_B, and the size of the pool) are highly relevant in the prediction of $O(v)$ and $W(v)$. The organ quality $Q(v)$ depends primarily on the weight of the patient. This is a consequence of the LKDPI metric that we use to measure transplant quality – transplants are deemed to be of higher quality if the donor-to-patient weight ratio is lower.

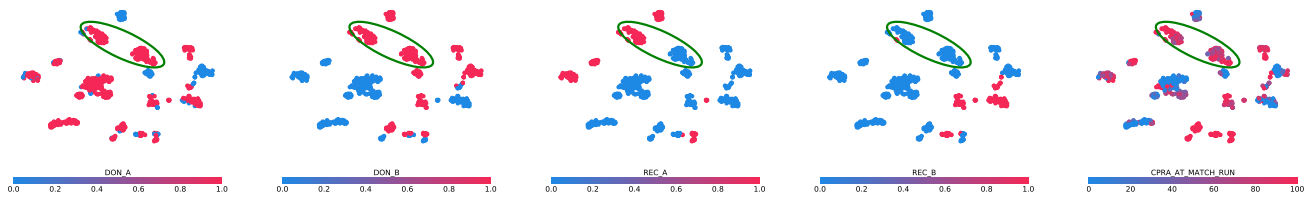


Figure 6: **Miscalibrated Explanatory Classes.** The two circled explanatory classes are matched with very high probability. Upon closer inspection, these classes correspond to highly sensitized difficult-to-match patients with easy-to-match donors.

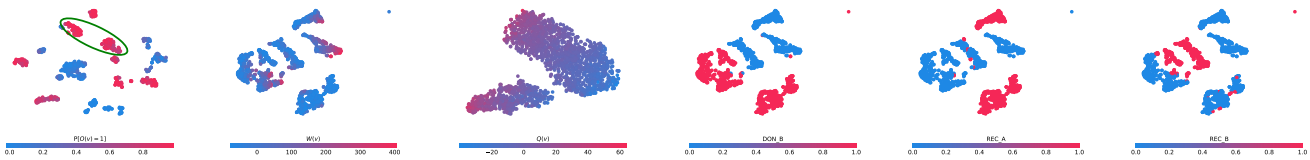


Figure 7: **t-SNE Projections and Explanatory Classes.** Using t-SNE, we project the SHAP values for $O(v)$, $W(v)$, and $Q(v)$ onto two dimensions revealing well-defined clusters, or explanatory classes. The classes for waiting time are clearly determined by blood type – specifically by the features DON_B, REC_A, and REC_B. Two miscalibrated classes for $O(v)$ are circled in green.

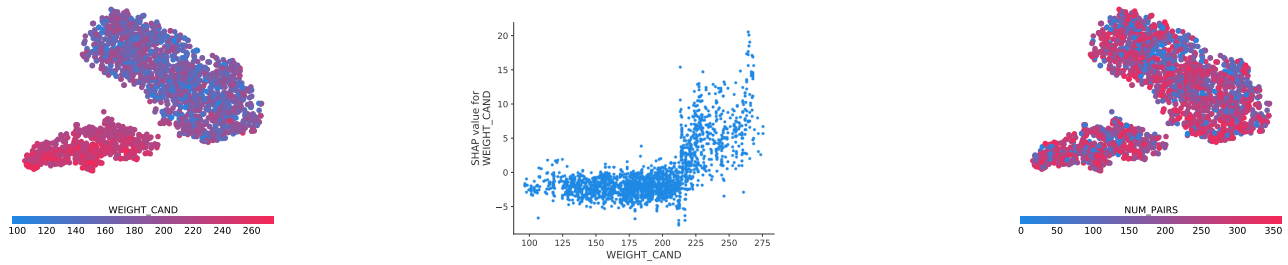


Figure 8: **Effect Groups for $Q(v)$** . On the left, we show how the patient’s weight varies across the TSNE-projected SHAP values. It is clear that the effect groups are distinguished by weight, with the heavier patients in the smaller left cluster. No other features determine the group – even the second ranked feature (shown on the right) is homogeneously mixed in both clusters. In the middle, we show how the feature importance for patient weight varies with its value. We can clearly see that for patients heavier than 210 pounds, the feature importance almost discretely shifts upwards – this shift corresponds to the point at which the effect group for the patient switches.

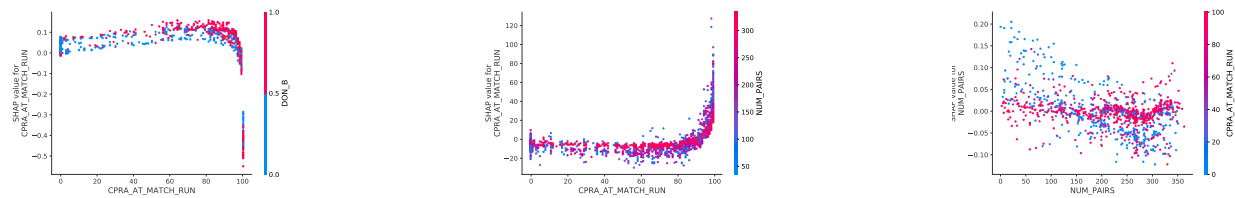


Figure 9: **SHAP Dependence Plots**. In the left two plots, we show the SHAP value for patient sensitivity (CPRA) for $O(v)$ and $W(v)$ respectively. On the right, we plot the interaction between the SHAP value for the size of the pool and patient CPRA in the prediction of $O(v)$. With the exception of exceedingly sensitized patients, we find that patients with higher sensitivity surprisingly are matched *more* frequently, and have a slightly *lower* waiting time. This effect is exacerbated when the patient’s paired donor is easy-to-match, and when the size of the pool increases. Indeed, we find that a large pool size tends to improve the probability of being matched for highly sensitized patients, but slightly *decreases* the probability of being matched for nonsensitive patients. These results all suggest that the ethical prioritization for moderately high CPRA patients is too strong.

Ethical statement

The economics, operations research, and AI communities have had substantial combined impact on the analysis, development, and fielding of real-world kidney exchanges (see, e.g. [Agarwal *et al.*, 2019; Biró *et al.*, 2019]). As discussed in Section 2, much of that work has focused on the development of sophisticated optimization techniques for maximizing efficiency (for various definitions of efficiency), and/or balancing efficiency with notions of fairness. Changing the allocation or matching policy of any system that connects needy participants with scarce resources inevitably results in necessary morally-laden decision-making, and with it a number of ethical implications.

In contrast, we view our line of research as a *complement* to that work, which seeks to redefine allocative systems; rather, we present a *decision support tool* that is meant to help stakeholders—primarily doctors, patients, and would-be donors—make their own informed decision regarding potentially life-and-death decisions. In that sense, one positive potential impact of our work is *increased agency*, especially of patients and donors who are part of notoriously opaque healthcare systems. Our tool also provides *increased transparency* into the matching process by applying techniques from the explainability literature. One potential negative implication could be the use of risk calculation by parties, such as insurance companies, that again seek to redefine allocative policies³. In the case of an insurance company, calculations of risk and expected reward compete to determine opportunities afforded to patients. While we believe, broadly, that access to more accurate estimates for, e.g., patient-, donor-, and patient-donor-specific waiting times and match qualities will globally benefit exchange participants, it is possible that those who are hard to match may be relatively harmed by an efficiency-optimizing insurance company. This downside can be mitigated by only allowing patients to request estimates, instead of making the tool publicly available.

³In our abstract, we mention that our tool can be used to help patients make insurance decisions: by providing patients with information about their predicted outcomes in kidney exchange, they can obtain a better understanding of their own prognosis, which can in turn help them select an insurance plan that works best for them. The risk calculation we discuss here is instead an optimization that occurs on behalf of an insurance company that aims to optimally price an insurance plan for a given patient.